



## OPEN Unravelling the luminescence spectrum of novel ceramic nucleus cultured pearl and the cause of its strong luster

Qing Su<sup>1,2</sup>, Yan Li<sup>1,2</sup>✉, Wei Shao<sup>2</sup> & Fanmiao Tang<sup>2</sup>

The newly developed ceramic-nucleus pearls employ ceramic materials for cultivation, differentiating from the traditional seashell-based nuclei. This innovation yields a product that resembles Akoya pearls but exhibits superior luster. In this manuscript, Energy Dispersive X-ray Fluorescence (EDXRF), three-dimensional (3D) fluorescence spectroscopy, photoluminescence (PL) spectroscopy, UV-visible (UV-vis) spectroscopy, Fourier Transform Infrared (FTIR) Spectroscopy, and Scanning Electron Microscopy (SEM) were used to thoroughly analyze the mother oyster of these ceramic-nucleus pearls. The test results suggest that these ceramic pearls may originate from the same mother oyster species as Akoya pearls, making them difficult to distinguish through visual observation. Nonetheless, the presence of abnormal characteristic peaks of Zr in EDXRF testing and additional weak emission centers observed at excitation/emission ( $E_x/E_m$ ) wavelengths of 292/346 nm in the 3D fluorescence spectra provide crucial evidence for differentiating between the two types of pearls. Furthermore, SEM analysis demonstrated that the nucleus and aragonite layer of the ceramic pearls are tightly bonded, with the aragonite layer that is distributed evenly and regularly. This structural feature may contribute significantly to the enhanced luster observed in ceramic pearls. The advent of ceramic-nucleus pearls opens new possibilities for improving the luster of cultured pearls, potentially revolutionizing the industry.

**Keywords** Ceramic pearls, Spectrum analysis, Fluorescence characteristics, Akoya pearl, Luster

Pearls are organic formations primarily composed of calcium carbonate, along with a small amount of organic matter. A lamellar stacking structure was formed by aragonite crystals and organic material<sup>1,2</sup>. Currently, the availability of natural pearls in the market is relatively limited, with the majority being cultured<sup>3</sup>. Extensive researches<sup>4–7</sup> which were focusing on various types and optimizing the identification characteristics of processed pearls have been conducted on these pearls by utilizing Raman spectroscopy, ultraviolet spectroscopy, and other methods. Shi et al.<sup>6</sup> investigated the identification features of Tahitian pearls. Fluorescence spectroscopy and Raman spectroscopy were employed by Zhou et al.<sup>4</sup> to detect Edison pearls that had undergone color treatment or fluorescence whitening, summarizing their identification techniques. The changes in fluorescence characteristics of akoya pearls following heat and light treatments were explored by Hiramats et al.<sup>1</sup>. Meanwhile, significant progress has been made in the innovations of pearl cultivation technology, particularly regarding to akoya pearls. Recent studies<sup>8,9</sup> have examined the sedimentation rates of pearl layers in akoya pearls cultivated along the eastern coast of Australia and the southwestern coast of India, with comparisons made to those produced in Japan. The relationship between the sex of mother oysters and the quality of cultured pearls was investigated by Iwai et al.<sup>10</sup> to enhance pearl quality. Additionally, Fukushima et al.<sup>11</sup> developed a novel method to suppress the immune system of akoya pearl oysters, successfully producing different types of pearls from these oysters. However, advancements in pearl cultivation technology predominantly focus on the cultivation location, the gender of the mother oyster, and the transplanted mantle, while relatively little research has been conducted on the nucleus of pearl cultivation.

Ceramic-nucleus pearls represent a new type of pearl that has recently emerged, its growth process is similar to that of ordinary pearls and the detailed cultured process of ceramic pearls is outlined in the supplementary materials. While they resemble Akoya pearls in appearance, a stronger luster is exhibited (specific proof can be found in the supplementary materials). In pearl valuation, luster is one of the most important criteria, which may enable ceramic pearls to be a new type of high-quality pearl. However, distinguishing the mother oyster

<sup>1</sup>Institute for Advanced Marine Research, China University of Geosciences, Guangzhou 511462, China. <sup>2</sup>Gemological Institute, China University of Geosciences, Wuhan 430074, China. ✉email: yanli@cug.edu.cn

used in the production of ceramic pearls based solely on appearance is challenging, and their similarity to ordinary pearls further complicates differentiation. Additionally, the underlying reason for their enhanced luster requires investigation, possibly linked to their unique ceramic nuclei and the structure of their pearl layers. This study explores a new method for cultivating superior pearls at a lower cost, demonstrating the feasibility and advantages of using ceramics as the nuclear material for pearl cultivation.

As technology continues to advance, a growing focus is placed on using non-destructive and rapid methods to detect and analyze pearls. Among these techniques, three-dimensional (3D) fluorescence and photoluminescence (PL) spectroscopy have emerged as some of the most commonly employed non-destructive testing methods<sup>12,13</sup>. These approaches allow for the assessment of pearl properties without causing any damage. Furthermore, scanning electron microscopy (SEM) is utilized in many studies to examine the intricate structure of pearl layers in detail<sup>5,14–16</sup>. By integrating these innovative techniques, not only is the identification of pearls enhanced, but a broader understanding of their structural characteristics is also contributed. From a gemological perspective, the first step in analyzing an unknown pearl sample is to determine its growth environment, followed by identifying the mother oyster that produced the pearl through various spectroscopic tests. Energy Dispersive X-ray Fluorescence (EDXRF) is an effective elemental analysis method for distinguishing whether the pearl originated in seawater or freshwater. 3D fluorescence spectroscopy and PL spectroscopy are used to identify the type of pearl based on the position of the fluorescence center and the intensity of the fluorescence background. Additionally, SEM is employed to investigate the relationship between the strength of pearl luster and the arrangement of aragonite layers. Therefore, this article explores the growth environment of ceramic pearls and identifies the mother oysters through a series of analyses, including EDXRF, 3D fluorescence spectroscopy, PL spectroscopy, and UV-visible (UV-vis) spectroscopy. The unique spectral features that help distinguish ceramic pearls from ordinary pearls are summarized. To verify the nuclear components of ceramic pearls and investigate the reasons for their stronger luster, some samples were cut and analyzed using Fourier Transform Infrared (FTIR) Spectroscopy to study their nuclear components. Furthermore, the pearl layer structure of ceramic pearls with that of ordinary pearls was also compared to explore the reasons behind their superior luster (Fig. 1).

## Results

### EDXRF analysis for the layers of novel ceramic-nucleus cultured pearls and reference samples

Through EDXRF testing conducted on nine samples in this study, it can be effectively determined whether samples P1 to P5 are seawater or freshwater pearls. The test results are presented in Fig. 2; Table 1. The Sr/Ca ratio for these samples was obtained by integrating the areas of the Ca and Sr peaks in the plotted curves. The Sr/Ca values for all samples P1 to P5 exceed 0.3 (Table 1) and based on previous research<sup>17,18</sup> it can be inferred that these samples are seawater pearls.

Notably, with the exception of P3, the ceramic pearl samples (P1 to P5) exhibited stronger Zr peaks compared to the ordinary pearl samples (E1, A1, T1, G1), with their intensity even surpassing that of the Sr peaks (Fig. 2a) and this phenomenon was not observed in the ordinary pearls (Fig. 2b). This observation may be attributed to the fact that the nuclei of P1, P2, P4, and P5 consist of a silicate ceramic doped with Zr elements. The thin pearl layer allowed for X-ray penetration, which enabled the testing of the internal ceramic composition of nuclear, resulting in a pronounced Zr peak. This hypothesis requires further investigation. In contrast, the XRF data for P3 does not differentiate it from ordinary pearls, indicating a need for additional testing to confirm whether its nuclear is ceramic. In addition, the presence of Rh and Ru elements in the spectrum is attributed to the influence of the Rh target in the XRF light tube.

### Fluorescence characteristics of novel ceramic-nucleus cultured pearls and reference samples

Under long wavelength ultraviolet light, notable blue-white fluorescence was observed in both the ceramic pearl samples P1–P5 and A1. In contrast, the E1 exhibited slightly weaker fluorescence, while the T1 and G1 were virtually inert, demonstrating no fluorescence. The fluorescence photo of the samples under long wave ultraviolet light can be found in the supplementary materials (Fig. S1).

Although similar blue-white fluorescence can be observed between samples P1–P5 and A1 under long-wavelength ultraviolet light, the fluorescence characteristics at other excitation wavelengths were found to be less intuitively apparent, indicating that more advanced fluorescence spectroscopy techniques are necessary for further analysis<sup>12</sup>. Therefore, in this study, 3D fluorescence spectroscopy was employed as an effective and rapid method for distinguishing between distinct types of pearls, and testing was conducted on the nine pearl samples to analyze their fluorescence characteristics. Significant differences in luminescent centers were identified between samples P1–P5 and A1 when compared to the other three pearl samples (Fig. 3). Notably, the Edison pearl E1 displayed the strongest fluorescence intensity, with its fluorescence center located within the excitation and emission wavelength range of 284/340 nm, accompanied by a shoulder peak in the spectrum at an emission wavelength of 340 nm (Fig. 3g). In contrast, T1 and G1 exhibited relatively weak fluorescence intensity, with their fluorescence centers situated in the excitation and emission range of 284/335 nm (Fig. 3h, i). Research has shown that the fluorescence centers of T1, E1, and G1 originate from tryptophan and protein-related substances commonly found in pearls. This organic component emits a fluorescence peak at approximately 340 nm when excited with a wavelength of 284 nm, indicating that the organic components in the layers of T1, E1, and G1 are indeed tryptophan and protein related substances<sup>4</sup>.

Samples P1–P5, along with A1, were characterized by the presence of two fluorescence centers located at approximately 374/446 nm and 374/462 nm within the  $E_x/E_m$  range (Fig. 3a–f), which were distinctly different from those of the other three samples. The appearance of dual fluorescence peaks at 446 nm and 462 nm upon excitation at 374 nm is characteristic of humic acid luminescence<sup>19</sup>. This indicates that the primary organic components of samples P1–P5 and A1 include humic acid, distinguishing them from other samples. The presence of humic acid may lead to the fluorescence quenching of amino acids, such as tryptophan. The greater the

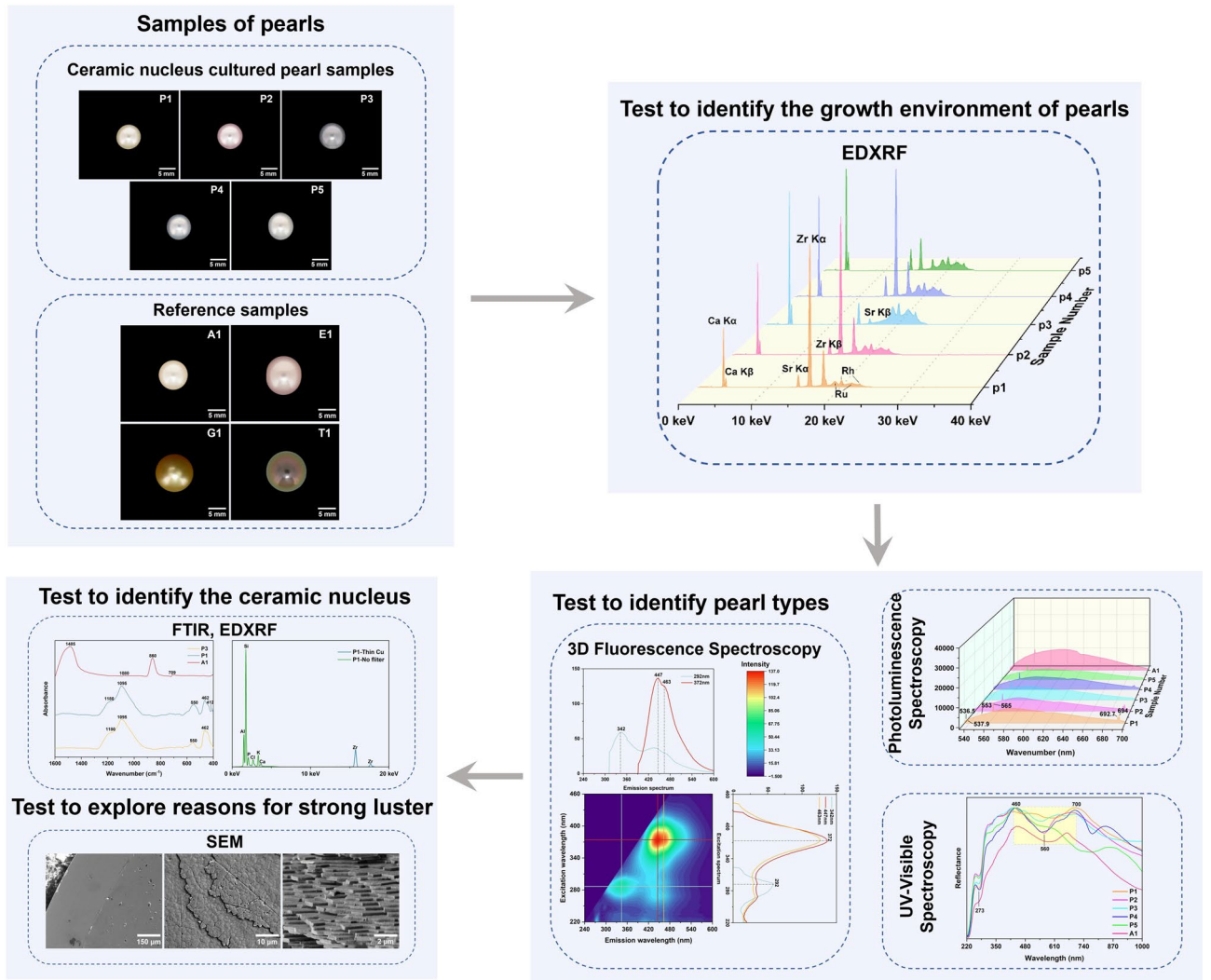


Fig. 1. Flowchart of novel ceramic pearl analysis and testing.

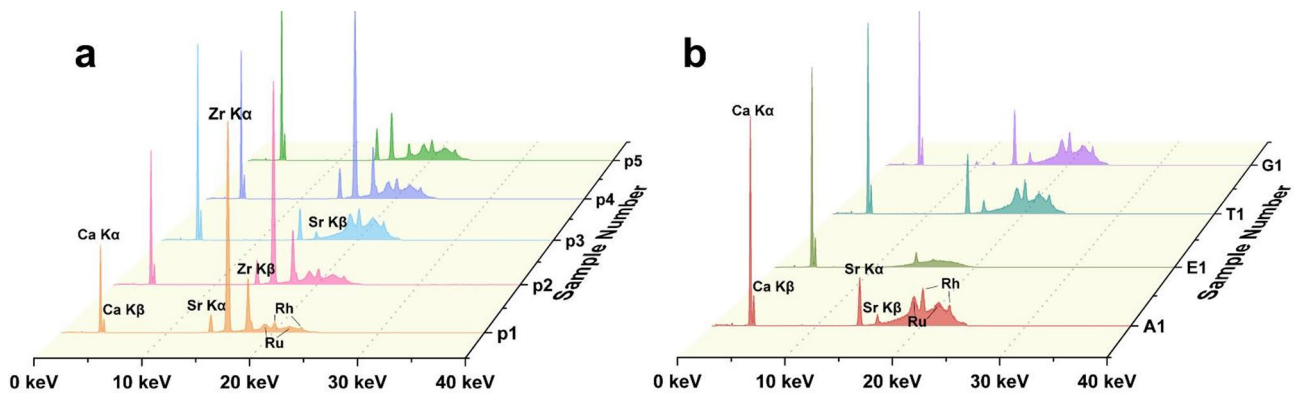


Fig. 2. EDXRF spectra of (a) novel ceramic-nucleus cultured pearl samples P1-P5 and (b) reference samples G1, T1, E1, A1.



concentration of humic acid, the more pronounced the fluorescence quenching phenomenon becomes<sup>20</sup> which leading to the weaker tryptophan luminescence of P1-5 and A1. Therefore, it can be concluded that the pearl oysters producing P1-P5 are consistent with those that produce Akoya pearls.

While P1-P5 and A1 share similarities in their fluorescence centers, certain differences were also observed; specifically, P1-P5 exhibited a fluorescence peak at approximately 346 nm when excited at 292 nm (Fig. 3a-e), whereas A1 displayed a very weak fluorescence peak at this wavelength that was nearly undetectable (Fig. 3f). This indicates that P1-P5 contains less humic acid than A1. Meanwhile, the fluorescence intensity of samples P1-P5 was generally weaker than that of A1. All of these differences may serve as key evidence supporting the presence of a ceramic nucleus in samples P1-P5.

#### PL spectroscopy analysis of novel ceramic-nucleus cultured pearls and reference samples

An analysis of the PL spectra of samples P1-P5 to further investigate their pearl types and distinguish them from ordinary pearls is also incorporated in this paper (Fig. 4). To ensure the accuracy of the analysis, the research method employed by previous researchers was imitated in order to identify pearls with similar appearances. Researchers have calculated the F/A ratio to evaluate the fluorescence background intensity and serve it as evidence for identification<sup>13</sup>. The F/A ratio is the total fluorescence (F) divided by the intensity of aragonite main peak at 565 nm (A) (Table 2).

The fluorescence background intensity of samples P1-P5 was found to be stronger than that of E1, yet significantly weaker than that observed in T1 (Fig. 4a-b), leading to the conclusion that P1-P5 cannot be classified as either Tahitian pearls or Edison pearls. The spectral shape of P1-P5 was determined to be similar to that of A1 and G1, which exhibits a strong aragonite peak at 564 nm, accompanied by an additional peak at 553 nm. The spectral shape of P1-P5 was determined to be similar to that of A1 and G1, which exhibits a strong aragonite peak at 564 nm, accompanied by an additional peak at 553 nm. This corresponds to the symmetric stretching vibration of  $\text{CO}_3^{2-}$  at  $1086\text{ cm}^{-1}$  and the in-plane bending vibration of  $\text{CO}_3^{2-}$  at  $701, 705\text{ cm}^{-1}$  in Raman peaks of the aragonite crystal<sup>9</sup>. And there are two very weak peaks at 536.4 and 537.9 nm, which are

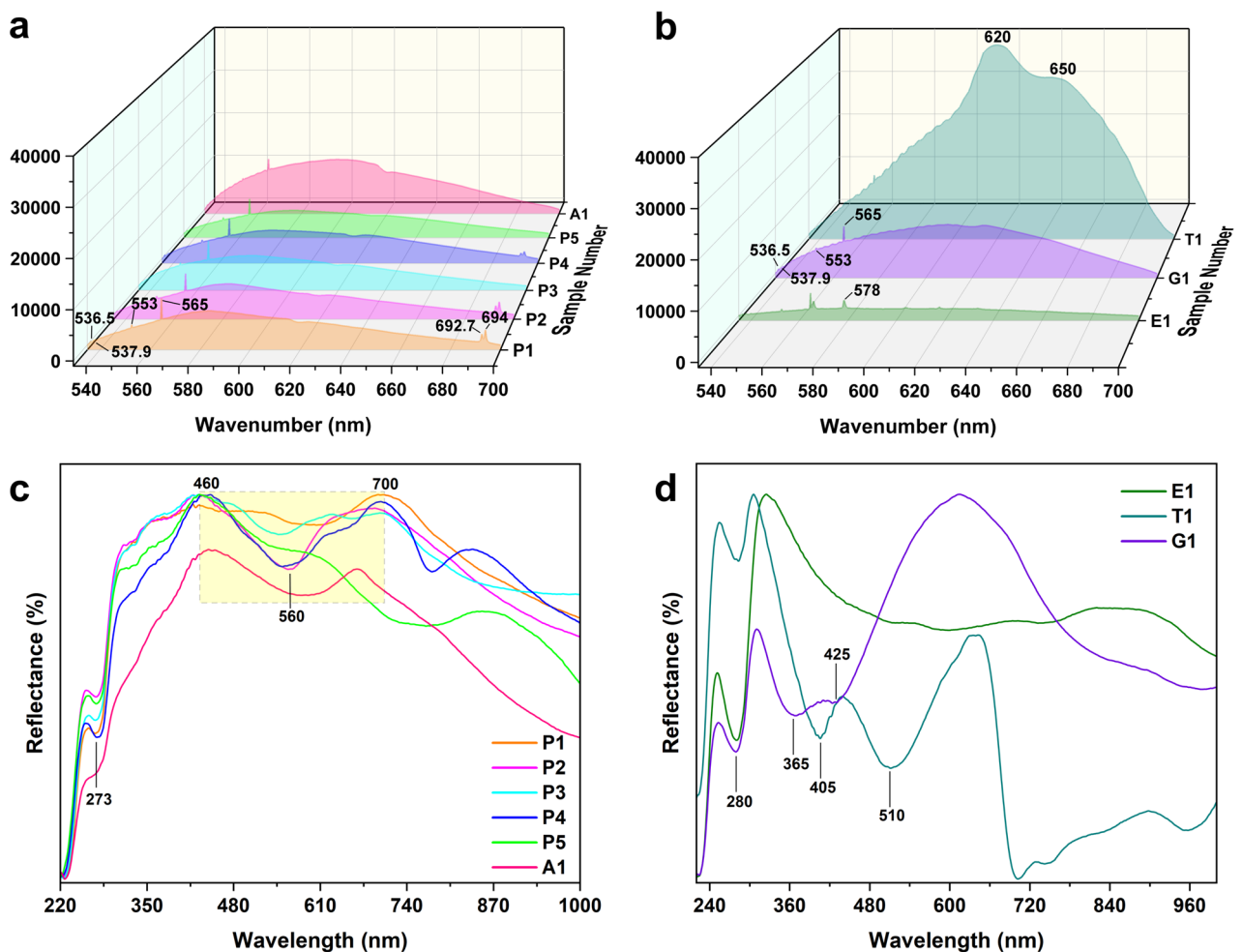


**Fig. 4.** PL spectrum of (a) novel ceramic-nucleus cultured pearl samples P1-P5, reference sample A1 and (b) other reference samples E1, G1, T1; UV-Vis reflectance spectra of (c) novel ceramic-nucleus cultured pearl samples P1-P5, reference sample A1 and (d) other reference samples E1, T1, G1.

Samples	F/A
P1	1.65
P2	1.77
P3	1.50
P4	1.70
P5	1.46
A1	4.74
G1	3.16
T1	37.43
E1	0.52

**Table 2.** The F/A of novel ceramic-nucleus cultured Pearl samples P1-5 and reference sample A1, G1, T1, E1.

speculated to correspond to weak aragonite lattice modes located at 155 and 208  $\text{cm}^{-1}$  in the Raman spectrum<sup>15</sup>. Further analysis revealed that the F/A values for P1-P5 range from 1 to 2, whereas the F/A values for A1 and G1 are 4.74 and 3.16. However, the spectral shape of P1-P5 was more closely resembles that of A1. Moreover, peaks at 692.7 nm and 694 nm were observed in samples P1, P2, and P4, consistent with the luminescence double peaks produced by the  ${}^2E \rightarrow {}^4A_2$  transition of  $\text{Cr}^{3+}$  in weak crystal fields<sup>21,22</sup>. Thus, it is speculated that trace amounts of  $\text{Cr}^{3+}$  may be present in P1, P2, and P4. Based on prior analyses of the 3D fluorescence spectra, a conclusion can be drawn that samples P1-P5 do not belong to the category of golden pearls from the South Sea. In summary, the PL spectrum provides further confirmation that P1-P5 can be classified as Akoya pearls, which possess unconventional nuclei.

### UV-Vis Reflectance spectra of novel ceramic-nucleus cultured pearls and reference samples

The UV-vis reflection spectra of all ceramic pearl samples demonstrated relatively consistent spectral peaks and samples P1-P5 exhibited absorption peaks at 273 nm, which were found to be similar to those of A1 (Fig. 4c). In contrast, T1, G1 and E1 exhibited absorption peaks at 280 nm (Fig. 4d). Previous study<sup>23</sup> have indicated that absorption peaks around 280 nm are commonly associated with organic compounds present in pearls which can induces biogenic aragonite mineralization, and most of them are a mixture of proteins and polysaccharides<sup>24</sup>. The absorption peaks of P1-5 and A1 at 273 nm are also attributed to organic compounds and the composition of these organic compounds differs from that of E1, T1, and G1 which may lead to a blue shift in the 280 nm absorption peaks. This finding is similar with the analysis derived from the 3D fluorescence spectra.

A detailed analysis of the UV-vis spectra for each sample indicated that G1 displays strong absorption peaks at 365 nm and 425 nm, while T1 demonstrates significant absorption at 400 nm and 510 nm, although its overall absorption intensity is notably weaker than that of the other samples. The strong absorption of the G1 sample at 365 nm in the purple region is attributed to a natural pigment, which contributes to its yellow color. And the absorption peak at 425 nm is likely due to organic compounds on the pearl's surface<sup>5</sup>. The absorption characteristics observed at 405 and 510 nm in T1 are distinctive features of natural Tahitian pearls. Studies have shown that the 405 nm feature is attributed to uroporphyrin pigmentation, while the 510 nm feature may be associated with a porphyrin<sup>24</sup>. Aside from the characteristic organic absorption peak at 280 nm, the overall absorption curve for E1 appeared relatively flat, lacking additional distinctive absorption peaks. When comparing P1-P5 with A1, it became evident that they exhibit a broad, gradual absorption band centered around 560 nm, extending from approximately 460 nm to 700 nm, with high degrees of similarity observed in their overall curves. The position of the absorption band varies slightly with different accompanying colors, which is believed to be due to the presence of a small amount of various chromogenic porphyrins in P1-P5 and A1<sup>12</sup>.

### FTIR and EDXRF spectra of the nucleus of pearl A1, P3 and P1

To further confirm the composition of the pearl nucleus in samples P1-P5, EDXRF tests (Fig. 5a-c) and FTIR spectroscopy (Fig. 5d) and were conducted on the nuclei of sample A1, P3 and P1, which was cut open. To better analyze the elemental composition of the ceramic nuclei and confirm the source of Zr, two different testing conditions were employed for EDXRF (Fig. 5a-c). The nuclear of a regular pearl typically consists of a seashell, the EDXRF analysis reveals Ca as the primary element in the nuclear of A1 (Fig. 5a). The FTIR spectrum of the nuclear of A1 exhibits a strong aragonite peak at 1485, 1080, 860 and 709  $\text{cm}^{-1}$  which represent asymmetric extension, symmetric extension, out of plane bending, and in-plane bending vibration modes of C-O respectively<sup>25</sup> (Fig. 5d). The spectrum of A1's nuclear shows the common feature of the  $\text{CO}_3^{2-}$  detected in seashells<sup>26</sup> suggesting that the nuclear of A1 is seashell.

A significant amount of Si and Al was detected in the EDXRF test for the nuclei of P3 and P1, alongside small amounts of K and Ca (Fig. 5b). This elemental composition closely resembles that of silicate ceramics, which typically consist of clay minerals, feldspar, and quartz. The primary elements found in these materials are aluminum, silicon, potassium, and calcium<sup>27</sup>. However, in addition to elements such as Si, Al, and K, there is a significant presence of Zr in the nuclear of P1, which suggests that the nuclear of P1 is a Zr-doped silicate ceramic (Fig. 5c). The FTIR spectrum results of the nuclear of P1 closely resemble those of P3. The FTIR spectrum of the nuclei of P3 and P1 reveals clear absorption peaks at around 1090  $\text{cm}^{-1}$  and 1180  $\text{cm}^{-1}$ . The peak at around 1090  $\text{cm}^{-1}$  corresponds to the stretching vibration of Si = O, while the peak at around 1180  $\text{cm}^{-1}$  represents the asymmetric stretching vibration of Si-O-Si. And the peak located at 462  $\text{cm}^{-1}$  is often attributed

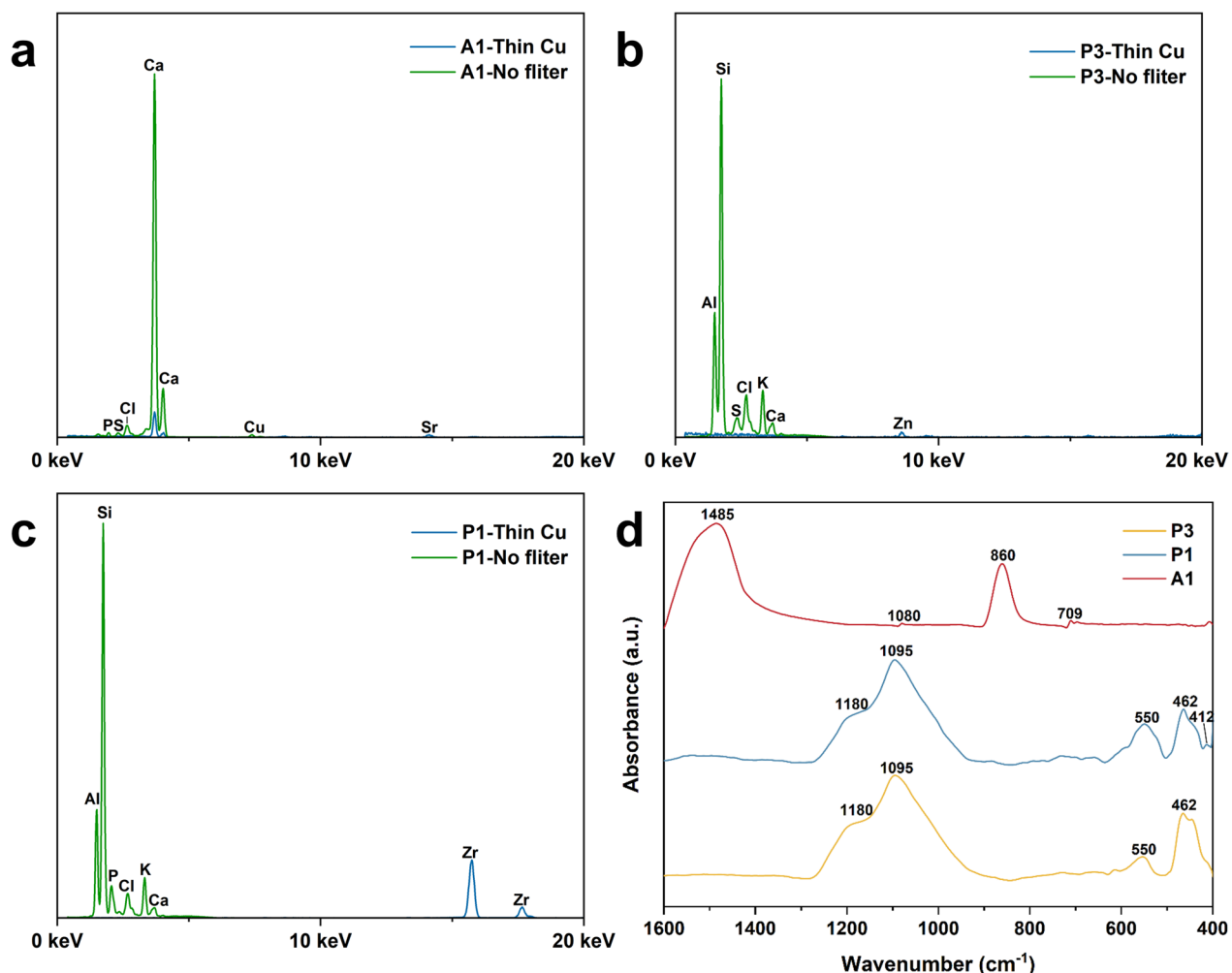


**Fig. 5.** (a–c) EDXRF spectra for the nucleus of A1, P3 and P1; (d) FTIR spectra of the cross-section area of the nucleus of A1, P3 and P1.

to the bending vibration of Si-O (Fig. 5d)<sup>28,29</sup>. These predominant peaks indicate that the nuclei are composed of silicate minerals. Furthermore, another evidence for the presence of Zr in the ceramic nuclear of P1 is that the peaks at 418 cm<sup>-1</sup> in its infrared spectrum are attributed to the stretching vibrations of Zr-O<sup>29</sup>. In summary, it can be concluded that the nuclei of samples P3 and P1 are ceramic. The presence of a significant amount of Zr in the nuclear of sample P1 supports the notion that the Zr detected in the EDXRF tests of the intact pearl samples P1, P2, P4, and P5 originates from the nucleus. Therefore, it can be inferred that the pearl samples P1 to P5 all have ceramic as their nuclei, and the reason the nuclear component was detected by EDXRF may be due to the thin layers that allow X-rays to penetrate more easily.

### SEM analysis of akoya pearl A1 and ceramic Pearl P3, P1

Based on the preceding analysis, it may be concluded that ceramic pearls can be classified as Akoya pearls that possess unconventional nuclei and stronger luster. The strength of pearl surface luster is demonstrated by the reflectivity of visible light. The argument for the luster strength of A1 and ceramic pearls can be found in the supplementary materials. As incident light propagates through pearl layers, the denser the aragonite crystal structure of a pearl layer, the weaker its refractive ability. As a result, more light is reflected from the surface of the pearl, leading to higher reflectivity<sup>30</sup>. Previous studies have mentioned that research on pearl luster focuses on two aspects: surface steps and aragonite layers within the cross-section of pearls<sup>31</sup>. Therefore, to explore the reasons behind the strong luster of ceramic pearls, it is essential to examine the structure of aragonite crystals within the pearl layers.

Samples A1, P3 and P1 were selected for further examination using SEM techniques. Upon cutting samples A1, P3 and P1, it was observed that the nuclei of P3 and P1 consists of hollow ceramic material, whereas the nucleus of A1 is composed of ordinary seashell material. Furthermore, optical photographs were taken of the surfaces of A1, P1 and P1 following cutting, as well as fresh cross-sectional images post-crushing (Fig. S2). SEM measurements were performed on both the cross-sectional and surface areas in order to examine the differences in pearl layer thickness, the structure of the surface aragonite layer, and the arrangement of aragonite within the

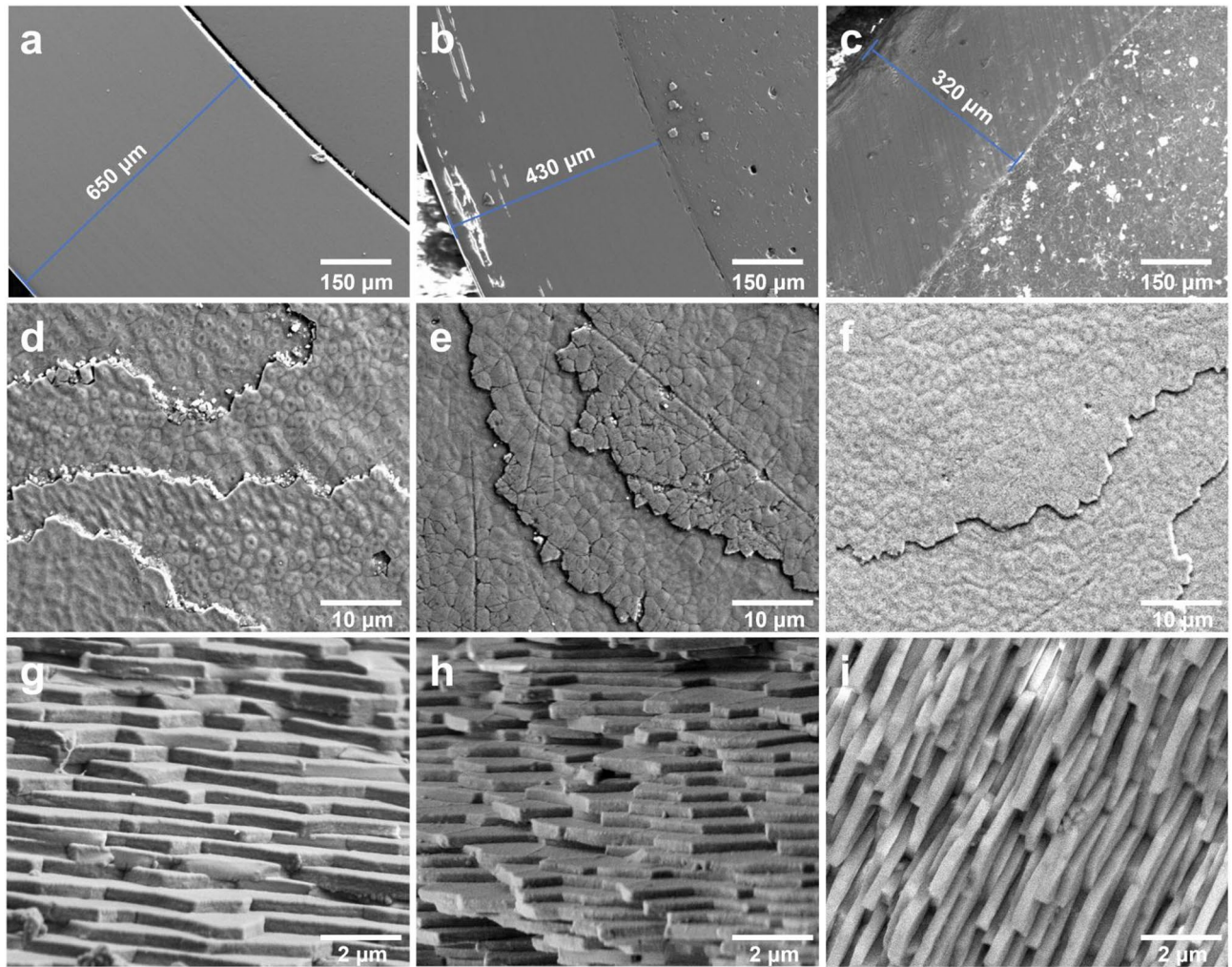


**Fig. 6.** SEM images of the pearl layer thickness of A1, P3 and P1 (a–c), SEM images of the surface structure of A1, P3 and P1 pearl layers (d–f), SEM images of the cross-section of A1, P3 and P1’s pearl layer (g–i).

cross-section of ceramic pearls as compared to ordinary Akoya pearls. Additionally, Energy Dispersive X-ray Spectroscopy (EDS) analysis was performed on both the pearl layer and the nucleus of P1, further demonstrating that Zr originates from the bead core rather than the bead layer. For detailed analysis, please refer to the supplementary materials.

The first set of tests focused on determining the thickness of the pearl layers, calculated by averaging measurements taken at three distinct positions on A1, P3 and P1. The results indicated that the layer thickness for A1 was approximately 0.65 mm (Fig. 6a), while P3 measured around 0.43 mm (Fig. 6b). And the layer thickness of P1 is only 0.32 mm (Fig. 6c). This finding suggests that A1 has a thicker pearl layer compared to that of P3 and P1, with P3’s thickness being comparable to that of most typical Akoya pearls, but the layer of P1 is thinner. Furthermore, the pearl layer of A1 was found to be not tightly bound to the nucleus following the sample cutting, in contrast to P3 and P1, which displayed a tight adhesion that made separation difficult.

This difference can be attributed to the large particle structure and rough surface of the ceramic nucleus. Common silicate ceramics typically have a heterogeneous structure with numerous pores<sup>32</sup>. The nuclei of P1 and P3 contain pores which may create mechanical interlocking with these pores, resulting in a strong bond between the pearl layers and the nuclei<sup>33</sup>. Additionally, the surface roughness of the heterogeneous ceramic structure is relatively high, which can be seen from the unevenness of the boundary between the pearl layers and nuclei. According to the formula:

$$f = \mu \times F_n$$

where  $f$ ,  $\mu$ ,  $F_n$  represent friction force, sliding friction coefficient, and positive pressure respectively. A higher friction coefficient means that it is more difficult for relative motion to occur when an external force is applied. This explains why P1 and P3 did not exhibit layer-nuclear separation during the cutting process, in contrast to A1, which was able to easily separate the nucleus from the layer. In conclusion, it is clear that the nucleus and

layer of ceramic pearls are more tightly bound than those of ordinary Akoya pearls, which could facilitate better bonding of the pearl layer and contribute to the enhanced luster observed in ceramic pearls.

The examination of the pearl layer structures on the surfaces of A1 and P3 revealed distinct contour-like growth patterns on both surfaces. The edge of the aragonite layer on the A1 surface exhibited significant cracking, characterized by the presence of numerous irregular hexagonal aragonite formations, with some areas displaying indistinct hexagonal features (Fig. 6d). In contrast, the hexagonal aragonite on the P3 and P1 surface demonstrated a clear and relatively flat morphology, characterized by regular shapes and fewer fractures (Fig. 6e–f). From the perspective of surface bead layer structure, it is evident that the structures of P3 and P1 are superior to that of A1.

Additionally, the unpolished cross-sections of the two pearl samples were analyzed, revealing similarities in the distribution of aragonite flakes, characterized by a dense structure, orderly distribution, and relatively flat fracture surfaces. However, it was noted that the A1 pearl layer exhibited a more uniform thickness, with an average measurement of 0.43  $\mu\text{m}$  (Fig. 6g). In contrast, the thickness of the P3 and P1 varied between 0.35  $\mu\text{m}$  and 0.55  $\mu\text{m}$  (Fig. 6h–i).

Overall, the characteristics of the pearl layer indicate that the structures of P3 and P1 are superior to that of A1, resulting in a brighter luster for the ceramic pearls. This section analyzes the mechanism of the strong bonding between the pearl layer and the ceramic nuclear from the perspectives of ceramic structure and surface roughness, demonstrating the reasons behind the enhanced luster of ceramic pearls from the perspective of gemology. This analysis reveals that, compared to pearls produced with ordinary seashells, those made with ceramic nuclei exhibit a significantly stronger luster. And the thickness of the pearl layer correlates with the cultivation time of pearls, suggesting that using ceramics as the nuclei can produce pearls with greater luster in a shorter growth cycle.

## Discussion

The novel ceramic-nucleus pearls, developed through emerging technologies, closely resemble traditional Akoya pearls in appearance but exhibit superior luster, which can be identified via advanced characterization techniques such as EDXRF, 3D fluorescence spectroscopy, PL spectroscopy, UV-vis spectroscopy, FTIR spectroscopy, and SEM. These tests have confirmed that the mother oysters used for cultivating ceramic pearls are the same as those used for akoya pearls (*Pinctada martensii* oyster). And the key characteristics for differentiating ceramic pearls from traditional akoya pearls can be found in the following results. EDXRF testing revealed unusually strong characteristic peaks of Zr in the ceramic pearls. Additionally, the 3D fluorescence spectra indicated that the fluorescence of ceramic pearls is generally weaker than that of akoya pearls, with a weak fluorescence center identified in the  $E_x/E_m$  range of 292/346 nm. To further investigate the reasons for the stronger luster of ceramic pearls, SEM analysis was conducted on the thickness, surface, and cross-section of the pearl layer. From the perspectives of ceramic structure and surface roughness, the strong bonding mechanism between the pearl layer and the ceramic nuclear is analyzed, proving that the strong luster of ceramic pearls originates from the use of ceramic nuclei, which facilitates the tight bonding of layer and nuclei as well as the uniform growth and distribution of nacre layers. Additionally, the thinner pearl layer of ceramic pearls reflects their advantages of shorter cultivation time and lower cost. In summary, cultivating pearls with a ceramic nucleus may be an effective method for enhancing pearl luster, potentially revolutionizing the cultured pearl industry.

## Materials and methods

### Samples

Five novel ceramic-nucleus cultured pearls (P1–P5), along with reference samples including Tahitian pearl, Edison pearl, Akoya pearl, and golden pearl from the South Sea, were selected for investigation. Sample photos and appearance descriptions are available in the supplementary materials (Figs. S3–S5).

### Characterization techniques

**EDXRF Spectroscopy.** Using a Thermo ARL Quant'x EDXRF Analyzer. The test condition for the pearl layers of intact pearls is using thick Pd as the filter, with a maximum voltage set at 28 kV under vacuum conditions, and each test was conducted for a duration of 60 s. Due to the inconsistent optimal detection conditions for Al and Zr, two different testing conditions were employed to better investigate the composition of the A1, P1 and P3 nuclei that have been cut open. Each test is conducted under vacuum conditions, lasting 60 s, one at a maximum voltage of 6 kV without using a filter, and the other at a maximum voltage of 40 kV, also for 60 s, with a thin Cu filter applied.

**3D fluorescence spectroscopy.** 3D fluorescence spectroscopy of intact pearl samples (P1–5, A1, T1, E1, G1) was conducted using a Jasco FP-8500 spectrofluorometer equipped with a xenon lamp. The parameters included an excitation bandwidth of 5 nm and an emission bandwidth of 2.5 nm, with an excitation range of 220–500 nm (with a 2 nm interval) and an emission range of 240–600 nm (with a 1 nm interval). A test voltage of 300 V and a scanning velocity of 1,000 nm/min were employed.

**PL Spectroscopy.** Measurements of intact pearl samples (P1–5, A1, T1, E1, G1) were carried out using a JASCO NRS7500 Raman spectrometer. Spectra were recorded using a 532 nm laser, about 4.7 mW laser power on the sample, a MPLFLN 20x objective lenses and a L600/B500nm diffraction grating. The slit area was  $100 \times 1000 \mu\text{m}$  resulting in a spectral resolution of  $9.61 \text{ cm}^{-1}$ . Spectra were acquired between 535 and 700 nm, with integration time of 5 s and the integration performed twice.

**UV-vis Spectroscopy.** UV-Vis spectra were obtained using the reflection method, due to the low transmittance of pearls. Measurements of intact pearl samples were conducted with a UV-vis spectrophotometer (Gem UV-100, Tianrui, China) over a scanning range of 220–1000 nm, with an integration time of 100 ms. The instrument

was calibrated to 100% reflectance using a reference white board. The light sources used are tungsten lamps and deuterium lamps, while the detector employed is an FFT-CCD detector.

**FTIR Spectroscopy.** Place the half-cut pearl samples (A1, P3, and P1) with their nuclei facing down on an iron plate featuring small holes with a radius of approximately 0.5 cm, allowing infrared light to pass through the holes and test the pearl nuclei. The main components of pearl nuclei were analyzed using a Bruker Vertex 80 Fourier transform infrared spectrometer and a detector operating in the light source in the mid-infrared to near-infrared range (7000–400  $\text{cm}^{-1}$ ). The objective lens of the instrument can achieve a magnification of up to 160 $\times$ . FTIR spectra were acquired in the range of 400–1600  $\text{cm}^{-1}$  with a resolution of 4  $\text{cm}^{-1}$  and by accumulating 64 scans.

**SEM.** Cut samples A1, P3 and P1 to small pieces, and a portion of A1, P3, P1 cross-sections was polished to test the thickness of the pearl layer, while the remaining portion was left unpolished to observe the arrangement of aragonite. Prior to testing, carbon spraying was applied to all samples. SEM analysis was conducted using a high-resolution field emission scanning electron microscope (Thermofisher Apreo 2 S). An acceleration voltage of 10 kV was used to examine the surface and thickness of the pearl layer, while an acceleration voltage of 2 kV was employed to analyze the unpolished cross-section. The working distance was maintained at approximately 10 mm.

## Data availability

Data will be made available on request. If someone wants to request the data from this study, please contact professor Yan Li at yanli@cug.edu.cn.

Received: 18 March 2025; Accepted: 2 June 2025

Published online: 01 July 2025

## References

- Hiramatsu, J., Iwahashi, Y. & Nagai, K. Heat- and light-treatment change the visible fluorescence of Akoya cultured pearls. *Fish. Sci.* **79**, 959–966 (2013).
- Micieli, D. et al. Characterizing pearls structures using X-ray phase-contrast and neutron imaging: A pilot study. *Sci. Rep.* **8**, 12118 (2018).
- Edeline, P. E., Leclercq, M., Le Luyer, J., Chabrier, S. & Droit, A. Pearl shape classification using deep convolutional neural networks from Tahitian Pearl rotation in *Pinctada margaritifera*. *Sci. Rep.* **13**, 13122 (2023).
- Zhou, C. H. et al. Detection of color treatment and optical brightening in Chinese freshwater edison pearls. *Gems Gemol.* **57**, 124–134 (2021).
- Yan, X. J. et al. The gemological characteristics of yellow seawater bead-cultured Pearl farming in Beihai city, Southern China. *Micron* **176** (2024).
- Shi, L., Wang, Y., Liu, X. & Mao, J. Component analysis and identification of black Tahitian cultured pearls from the oyster *Pinctada margaritifera* using spectroscopic techniques. *J. Appl. Spectrosc.* **85**, 98–102 (2018).
- Kiefert, L. & Karamelas, S. Use of the Raman spectrometer in Gemmological laboratories: Review. *Spectrochim. Acta A* **80**, 119–124 (2011).
- Kripa, V., Mohamed, K. S., Appukuttan, K. K. & Velayudhan, T. S. Production of Akoya pearls from the Southwest Coast of India. *Aquaculture* **262**, 347–354 (2007).
- Otter, L. M., Agbaje, O. B. A., Huong, L. T. T., Häger, T. & Jacob, D. E. Akoya cultured pearl farming in Eastern Australia. *Gems Gemol.* **53**, 423–437 (2017).
- Iwai, T., Takahashi, M., Ido, A., Miura, C. & Miura, T. Effect of gender on Akoya Pearl quality. *Aquaculture* **437**, 333–338 (2015).
- Fukushima, E. et al. A xenograft mantle transplantation technique for producing a novel Pearl in an Akoya oyster host. *Mar. Biotechnol.* **16**, 10–16 (2014).
- Li, Y. J., Chen, C. Y. F. & Li, L. P. Spectroscopy study of  $\gamma$ -ray irradiated Gray Akoya pearls. *Spectrosc. Spectr. Anal.* **43**, 1056–1062 (2023).
- Chen, C. Y. F. & Li, L. P. The application of photoluminescence spectra on identification of different types of pearls. *Spectrosc. Spectr. Anal.* **42**, 20–25 (2022).
- Satitkune, S. et al. Combination of FTIR and SEM for identifying freshwater-cultured pearls from different quality. *Opt. Spectrosc.* **120**, 500–504 (2016).
- Yan, X. J. et al. Unique spectral characteristics of natural-color edison pearls cultured in *Hyriopsis cumingii*, and its formation mechanisms. *Micron* **160** (2022).
- Edeline, P. E., Leclercq, M., Le Luyer, J., Droit, A. & Chabrier, S. 3D microscopic reconstruction of pearls using combined optical microscopy and photogrammetry. *Sci. Rep.* **14**, 14180 (2024).
- Sakakura, I., Tsuchida, H., Sasaki, Y. & Hayashii, H. Elemental analysis of cultured pearls by PIXE. *Int. J. PIXE* **27**, 93–99 (2017).
- Zhang, E., Huang, F. Q., Wang, Z. T. & Li, Q. Characteristics of trace elements in freshwater and seawater cultured pearls. *Spectrosc. Spectr. Anal.* **34**, 2544–2547 (2014).
- Li, Y. J. & Li, L. P. Application of Three-Dimensional fluorescence spectroscopy in Pearl detection: A case study of Gray Akoya Pearl. *J. Gems Gemmol.* **25**, 46–53 (2023).
- Wang, Z., Cao, J. & Meng, F. Interactions between protein-like and humic-like components in dissolved organic matter revealed by fluorescence quenching. *Water Res.* **68**, 404–413 (2015).
- Toyoda, T., Obikawa, T. & Shigenari, T. Photoluminescence spectroscopy of  $\text{Cr}^{3+}$  in ceramic  $\text{Al}_2\text{O}_3$ . *Mater. Sci. Eng. B* **54**, 33–37 (1998).
- Lewis, P. M., Keerthana, N., Hebbar, D., Choudhari, K. S. & Kulkarni, S. D.  $\text{Cr}^{3+}$  doped  $\text{Al}_2\text{O}_3$  nanoparticles: Effect of  $\text{Cr}^{3+}$  content in intensifying red emission. *Curr. Appl. Phys.* **32**, 71–77 (2021).
- Yan, J. et al. Study on the common effect of heat treatment, dyeing or irradiation treatment on UV-Vis diffuse reflectance spectra of pearls. *Spectrosc. Spectr. Anal.* **42**, 3697–3702 (2022).
- Jin, S. Y., Renfro, N. D., Palke, A. C., Ardon, T. & Homkrajac, A. Application of UV-VIS-NIR spectroscopy to gemology. *Gems Gemol.* **60** (2024).
- Lee, S. W., Jang, Y. N. & Kim, J. C. Characteristics of the aragonitic layer in adult oyster shells, *Crassostrea gigas*: Structural study of myostracum including the adductor muscle scar. *Evid. Based Complement. Altern. Med.* **2011**, 742963 (2011).
- Yarnpakdee, S., Senphan, T., Karnjanapratum, S., Jaisan, C. & Wangtueai, S. Structural characterization and antibacterial activity of Pearl oyster (*Pinctada maxima*) shell as affected by calcination temperature. *J. Agric. Food Res.* **19**, 101551 (2025).

27. Hmeid, H. A. et al. Preliminary characterization and potential use of different clay materials from North-Eastern Morocco in the ceramic industry. *Mater. Today Proc.* **58**, 1277–1284 (2022).
28. Partyka, J., Sitarz, M., Leśniak, M., Gasek, K. & Jeleń, P. The effect of  $\text{SiO}_2/\text{Al}_2\text{O}_3$  ratio on the structure and microstructure of the glazes from  $\text{SiO}_2\text{-Al}_2\text{O}_3\text{-CaO-MgO-Na}_2\text{O-K}_2\text{O}$  system. *Spectrochim. Acta A* **134**, 621–630 (2015).
29. Adamczyk, A. The study of the influence of  $\text{ZrO}_2$  precursor type and the temperature of annealing on the crystallization of the tetragonal polymorph of  $\text{ZrO}_2$  in Zirconia-Silica gels. *Gels* **8** (2022).
30. Li, Q., Zhang, E. & Tu, X. Q. Relationship between luster and microstructure of seawater cultured Pearl. *Acta Mineral. Sin.* **36**, 225–230 (2016).
31. Fu, F., Tian, L. G., Xu, X. G., Xu, S. & Hu, X. B. Influence of microstructure on optical behaviour of freshwater cultured pearls. *Mater. Res. Innov.* **18**, 245–250 (2014).
32. Falamaki, C., Afarani, M. S. & Aghaie, A. Initial sintering stage pore growth mechanism applied to the manufacture of ceramic membrane supports. *J. Eur. Ceram. Soc.* **24**, 2285–2292 (2004).
33. Zhang, L. et al. Porous  $\text{Si}_3\text{N}_4$  ceramics with surface roughness for bone repair. *Ceram. Int.* **50**, 7558–7566 (2024).

## Acknowledgements

This work was supported by Annual Key Project of Modern Public Visual Art Design Research Center - Research on the Protection, Inheritance and Innovation of Ancient Chinese Accessory Culture in the Digital Age (No.JD-2024-03), “CUG scholar” Scientific Research Funds at China University of Geosciences, Wuhan (No. CUG2022185), China Arts and Crafts Society 2024 Arts and Crafts Research Project, Case Study on the Development and Brand Building of Tianjin Silk Craft Industry (No. CNACS2024-I-3).

## Author contributions

Q.S.: Investigation, wrote original draft, analyzed and discussed the results. Y.L.: Date curation, investigation, analyzed and discussed the results. Y.S. and F.T.: Supervised the experiments. All authors have reviewed the manuscript.

## Declarations

### Competing interests

The authors declare no competing interests.

## Additional information

**Supplementary Information** The online version contains supplementary material available at <https://doi.org/10.1038/s41598-025-05370-w>.

**Correspondence** and requests for materials should be addressed to Y.L.

**Reprints and permissions information** is available at [www.nature.com/reprints](http://www.nature.com/reprints).

**Publisher's note** Springer Nature remains neutral with regard to jurisdictional claims in published maps and institutional affiliations.

**Open Access** This article is licensed under a Creative Commons Attribution-NonCommercial-NoDerivatives 4.0 International License, which permits any non-commercial use, sharing, distribution and reproduction in any medium or format, as long as you give appropriate credit to the original author(s) and the source, provide a link to the Creative Commons licence, and indicate if you modified the licensed material. You do not have permission under this licence to share adapted material derived from this article or parts of it. The images or other third party material in this article are included in the article's Creative Commons licence, unless indicated otherwise in a credit line to the material. If material is not included in the article's Creative Commons licence and your intended use is not permitted by statutory regulation or exceeds the permitted use, you will need to obtain permission directly from the copyright holder. To view a copy of this licence, visit <http://creativecommons.org/licenses/by-nc-nd/4.0/>.

© The Author(s) 2025